Geomechanics for Energy and the Environment 37 (2024) 100520

Contents lists available at ScienceDirect

Geomechanics for Energy and the Environment

journal homepage: www.elsevier.com/locate/gete

Modelling the thermo-mechanical behaviour of a rock joint

Thanh Son Nguyen [a,*], Olaf Kolditz [b], Jeoung Seok Yoon [c], Li Zhuang [d]

[a] Canadian Nuclear Safety Commission (CNSC), 280 Slater, Ottawa K1P 5S9, Canada
[b] Helmholtz Centre for Environmental Research (UFZ), Germany
[c] Helmholtz Centre Potsdam German Research Centre for Geosciences (GFZ), Germany
[d] Korea Institute of Civil Engineering and Building Technology (KICT), South Korea

ARTICLE INFO

Keywords:
Rock joint
Shear
Dilation
Thermal shearing
Viscoplasticity
Nuclear waste
Geological disposal

ABSTRACT

The CNSC, the Canadian regulator for the nuclear industry, participated in DECOVALEX-2023 Task G that focuses on the thermo (T) - hydro (H)- mechanical (M) behaviour of rock joints. Joints are omnipresent in rock masses and are planes of weakness in the host rock. When deep geological repositories (DGRs) for radioactive waste are being considered in areas where rock joints are present, the joints could be preferential pathways for radionuclide migration. Therefore, their THM behaviour must be better understood to assess the safety of the DGR. Under different possible internal and external perturbations, a joint can move by shear and dilation. If the joint crosses the emplacement area of a waste container, the heat generated from the waste can itself induce shearing of the joint. Excessive shear movement can in turn lead to failure of the container, resulting in earlier release of radionuclides. Furthermore, dilation that might accompany shear, results in an increase in the joint aperture creating a faster flow path for radionuclide transport. Mathematical models are important tools that need to be developed and employed, in order to assess joint shear and dilation under different loading conditions, such as the heat generated from the emplaced waste. The authors have developed such a mathematical model based on a macroscopic formulation within the framework of elasto-plasticity. It is verified against analytical solutions and validated against shear under constant normal load tests and thermal shearing tests of joints in granite.

1. Introduction

Discontinuities, which we call joints or fractures in this work, constitute planes of weakness and hydraulic conduits in rock masses and need special attention in the design and construction of underground structures. The joint behaviour under different thermal, hydraulic and mechanical processes and their combination needs to be understood for the safe and optimal operation of activities such as carbon geo-sequestration, geothermal energy extraction, and shale gas production[1–5]. The focus of this paper is on geological disposal of radioactive waste being considered in many countries which consists of emplacing the waste in a repository at depths of hundreds of metres in a suitable rock formation. A deep geological repository (DGR) relies on a multiple barrier system to contain the waste and isolate it from the surface environment for periods of hundreds of thousands to millions of years[6]. The main components of the multiple barrier system are the waste container, the bentonite sealing system that surrounds the container in the emplacement room and the host rock formation (Fig. 1a).

The primary type of waste considered for deep geological disposal is high-level radioactive waste, such as used fuel from nuclear power plants. High-level waste (HLW) generates heat and would substantially raise the ambient temperature in the DGR and host rock for tens of thousands of years. This heat results in complex multiphysical processes that perturb the Thermal (T)-Mechanical (M)- Hydraulic (H)- Chemical (C) regime in the multiple barrier system and impact its long-term performance [7,8]. In this paper, we focus on a scenario when a joint intersects the emplacement area of a container, as schematically illustrated in Fig. 1b. Several external events such as earthquakes or water recharge from future deglaciation, and internal processes such as the heat generated from the waste, can potentially trigger joint movement. Excessive shear slip is the most damaging joint movement since it can affect the structural integrity of the waste container, potentially resulting in earlier release of radionuclides. Shearing is usually accompanied by dilation resulting in an increase in the joint aperture and permeability, further enhancing its ability to transport radionuclides.

* Corresponding author.
E-mail address: son.nguyen@cnsc-ccsn.gc.ca (T.S. Nguyen).

https://doi.org/10.1016/j.gete.2023.100520
Received 19 July 2023; Received in revised form 24 November 2023; Accepted 24 November 2023
Available online 30 November 2023

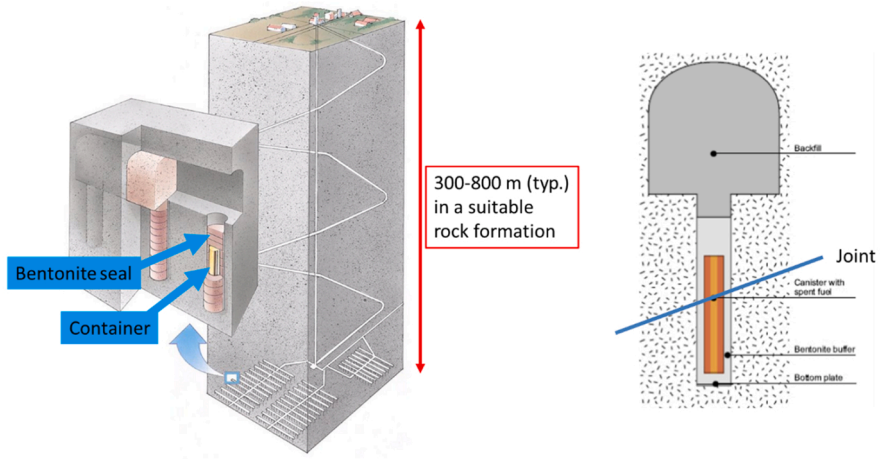

a) Generic arrangement of a DGR b) Joint crossing the area of an emplaced container

Fig. 1. Example of geological disposal concept (from[6]).

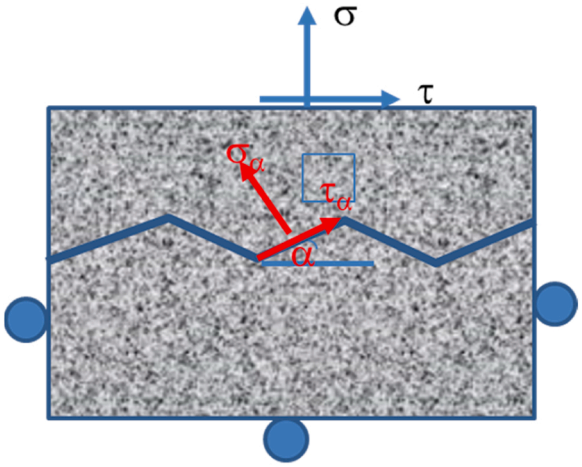

Fig. 2. Saw-tooth conceptualization of a rock joint.

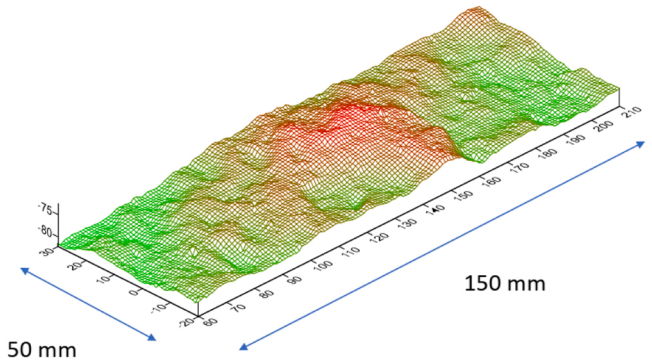

Fig. 3. Scanned surface of a joint in Freiberg granite (based on[23]).

The work being reported here is part of the Canadian Nuclear Safety Commission's contribution to task G of the DECOVALEX-2023 project (https://decovalex.org), an international collaborative project for the development and validation of models of coupled THMC processes in geological disposal systems. Task G of DECOVALEX-2023 focuses on THM processes of rock joints. The authors have developed a mathematical model that can be used to assess the scenario of thermoshearing of a joint in the vicinity of an emplaced waste container. The model is

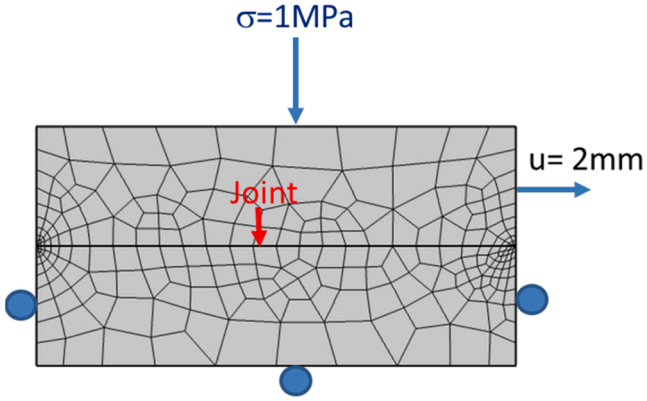

Fig. 4. Finite element model for joint shear under constant normal stress.

based on a macroscopic formulation within the framework of elasto-plasticity. It is verified against analytical solutions and validated against shear under constant normal load tests on jointed granite specimens. It is finally used to simulate thermal shearing tests of jointed granite specimens performed in the laboratory to further understand the processes that are relevant to the thermoshearing scenario considered in the safety assessment of DGRs for HLW.

2. Mathematical formulation

2.1. Viscoplastic formulation

Since the 1970s, many models were developed to predict the shear strength and displacement of rock joints e.g.[9–16]. It is not our intention to perform an in-depth review of these models. In task G of DECOVALEX-2023[17], different joint models have been developed in order to simulate thermoshearing problems using a set of well-designed experimental data. There are two main types of approaches adopted in the above models. The first approach is a microscopic one, in which the asperities of the scanned surfaces (e.g. Fig. 3) of the joint are exactly represented and assumptions are made about the interaction between these asperities. In this work, we adopted the second approach, which is the macroscopic one. The model that was developed requires input data on average joint characteristics that can be obtained from basic and inexpensive characterization techniques[13,19–21].

The proposed model is based on the saw-tooth conceptualization (Fig. 2) of Patton[9], and Plesha[10] and the elasto-plastic formulation by

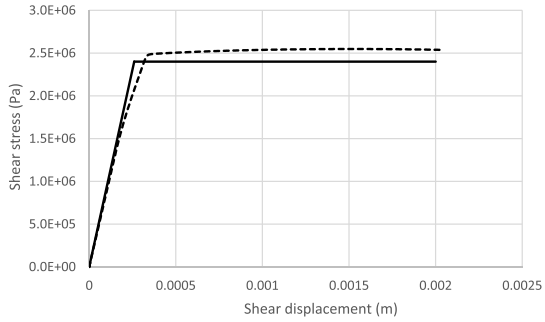

a) Shear stress evolution

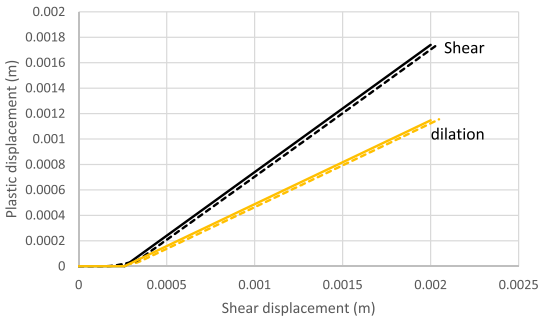

b) Evolution of plastic displacement (shear and dilation)

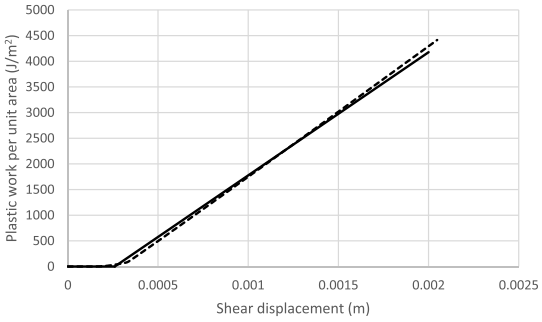

c) Evolution of plastic work (per unit area of joint surface)

Fig. 5. Verification of the joint model for shear under constant normal stress – *The dashed line represents the model results and the solid line the analytical solution.*

Table 1
Input data for modelling shear under constant normal load tests on jointed Freiberg granite.

Input parameter	Value	Source
Young's modulus of intact rock	50 GPa	[23]
Poisson's ratio of intact rock	0.2	Assumed
JRC	16	Estimated from joint profile (Fig. 3) from methodology described in[21]
JCS	120 MPa	Assumed equal to uniaxial compressive strength[23]
Joint degradation coefficient c	1.7e-4 m/N for 1 MPa normal stress, then 1e-5 m/N for subsequent normal stresses	Calibrated value
ks	9 GPa/m	calibrated
kn	Smooth step function from 0 at 0.5 μm dilation to 8740 GPa/m at 0.5 μm compression.	calibrated

Nguyen and Selvadurai[15]. According to that conceptualization, a global state of shear and normal stress τ and σ on the joint results in a local state of stress τ_α and σ_α on the joint asperity, inclined at an angle α with respect to the global shear direction.

From equilibrium consideration, the local stresses are related to the global stresses as follows:

$$\sigma_\alpha = (-\sigma \quad \sin\alpha + \tau \quad \cos\alpha) \quad \cos\alpha \tag{1}$$

$$\tau_\alpha = (\sigma \quad \sin\alpha + \tau \quad \cos\alpha)\cos\alpha \tag{2}$$

Joint slip starts when the friction resistance along the asperity is exceeded, ie. $|\tau_\alpha| \geq -\sigma_\alpha \tan\varnothing$, where ∅ is the friction angle along the asperity. In the framework of elastoplasticity, a yield criterion (using tension positive convention) that defines the onset of permanent deformation of the joint is then defined as:

$$F = |\sigma \quad \sin\alpha + \tau \quad \cos\alpha| + (-\sigma \quad \sin\alpha + \tau \quad \cos\alpha)\tan\varnothing \tag{3}$$

By imposing the constraint that only shear stress can produce permanent deformation[16], a plastic yield potential that determines the plastic strain rate is defined as:

$$Q = |\tau_\alpha| = |\sigma \quad \sin\alpha + \tau \quad \cos\alpha| \tag{4}$$

The stress-strain relationship for the joint is given by:

$$\begin{pmatrix} \tau \\ \sigma \end{pmatrix} = \begin{bmatrix} k_s & 0 \\ 0 & k_n \end{bmatrix} \begin{pmatrix} u - u_p \\ v - v_p \end{pmatrix} \tag{5}$$

Where:

u, v are the total shear and normal relative displacement [m] of the joint along the global directions.

u_p, v_p are the plastic shear and normal relative displacement [m] of the joint along the global directions.

k_s, k_n are the elastic shear and normal stiffness of the joint [Pa/m].

Using the viscoplastic formulation by Zienkiewicz and Cormeau[18], the rate of plastic relative displacement is given by:

$$\begin{pmatrix} \frac{du_p}{dt} \\ \frac{dv_p}{dt} \end{pmatrix} = \mu \left\langle \frac{F}{F_0} \right\rangle \begin{pmatrix} \frac{\partial Q}{\partial \tau} \\ \frac{\partial Q}{\partial \sigma} \end{pmatrix} = \mu \left\langle \frac{F}{F_0} \right\rangle \begin{pmatrix} \pm\cos\alpha \\ \pm\sin\alpha \end{pmatrix} \tag{6}$$

Where:

$\langle F/ \quad F_0 \rangle = 0$ if $F/F_0 < 0$; $\langle F/ \quad F_0 \rangle = F/ \quad F_0$ otherwise.

F_0 is a reference value of the yield function [Pa].

μ [1/s] is a "fluidity" constant (1/s) that determines the rate of the plastic displacement. When simulating purely plastic behaviour as in the present paper, this constant can be set equal to one.

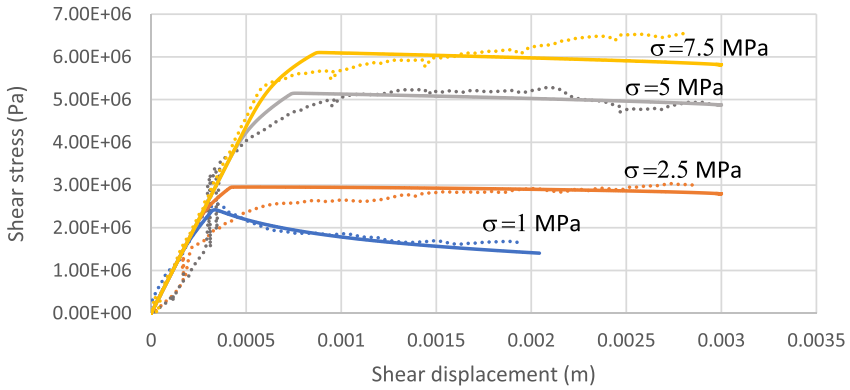

a) Shear stress vs shear displacement

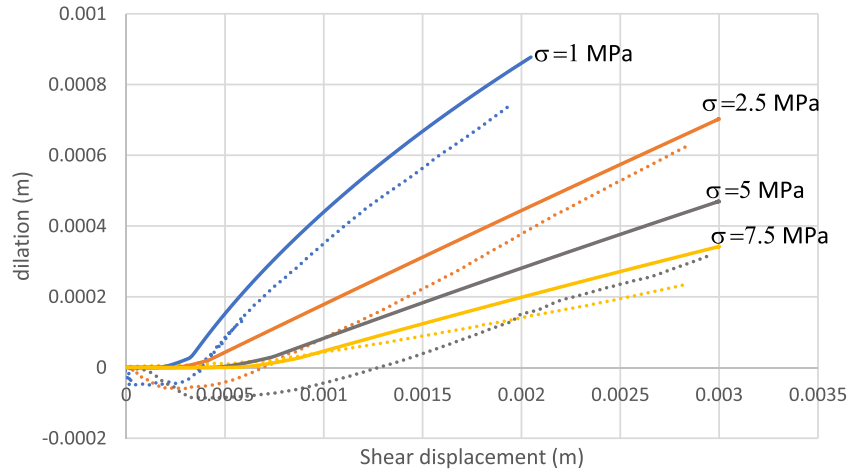

b) Dilation vs shear displacement

Fig. 6. Validation of the joint model with shear under constant normal stress tests for Freiberg granite. *Solid lines are modelling results; dotted lines are experimental values.*

Table 2
Input parameters for modelling of thermoshearing of fracture in Pocheon granite.

Input parameter	Value (model input/ measured)	Reference
Density – granite (kg/m3)	2609 /2609	[25]
Young's modulus – granite (GPa)	50 /50	[25]
Poisson's ratio – granite (-)	0.275/0.275	[25]
Thermal conductivity -granite (W/m/K)	2.2/1.96–2.2	[25]
Heat capacity – granite (J/kg/K)	645/645	[25]
Coefficient of linear thermal expansion – granite (1/K)	8e-6 (SF), 1e-5(TF)/6.24e-6	[25]
Shear stiffness – fracture (GPa/m)	750	calibrated
Normal stiffness - fracture (GPa/m)	8740	calibrated
JRC	0.66 (SF), 12.5(TF)/0.66 (SF), 12.5 (TF)	[25]
JCS (MPa)	120	calibrated
Joint friction angle ϕ (°)	31	[26]
Joint asperity angle α (°)	1.5 (SF), 9 (TF)	Eq. (9)
Joint degradation constant (m/N)	1e-6 (SF), 3e-4(TF)	calibrated

2.2. Model parameters

The joint model is fully described by Eqs. (4)–(6), and the required parameters are the elastic stiffness constants k_s, k_n, the friction angle ϕ and the asperity angle α. We propose that the above parameters be estimated from two index parameters widely used by rock engineers, the joint roughness coefficient (JRC) and the joint compressive strength (JCS). JRC and JCS are the key parameters of the Barton-Bandis shear strength criterion [13,19–21] for rock joints:

$$|\tau| + \sigma \quad \tan\left(JRC \quad Log_{10}\left(\frac{JCS}{\sigma}\right) + \varnothing\right) = 0 \tag{7}$$

JRC is an index that determines the roughness of the joint walls, while JCS is indicative of the strength of the joint walls. The determination of JRC, JCS could be performed by simple laboratory tests as detailed by Barton[21], who also proposed empirical expressions of the elastic stiffness constants k_s, k_n from JRC and JCS and a determination of the friction angle ϕ using the tilt test and the Schmidt hammer test. The asperity angle, which is specific to the present model, is determined as detailed below.

It is noted that the yield condition, Eq. (3), can be written as:

$$|\tau| + \sigma \, tan(\alpha + \varnothing) = 0 \quad when \; \sigma \sin\alpha + \tau \cos\alpha > 0 \tag{8.a}$$

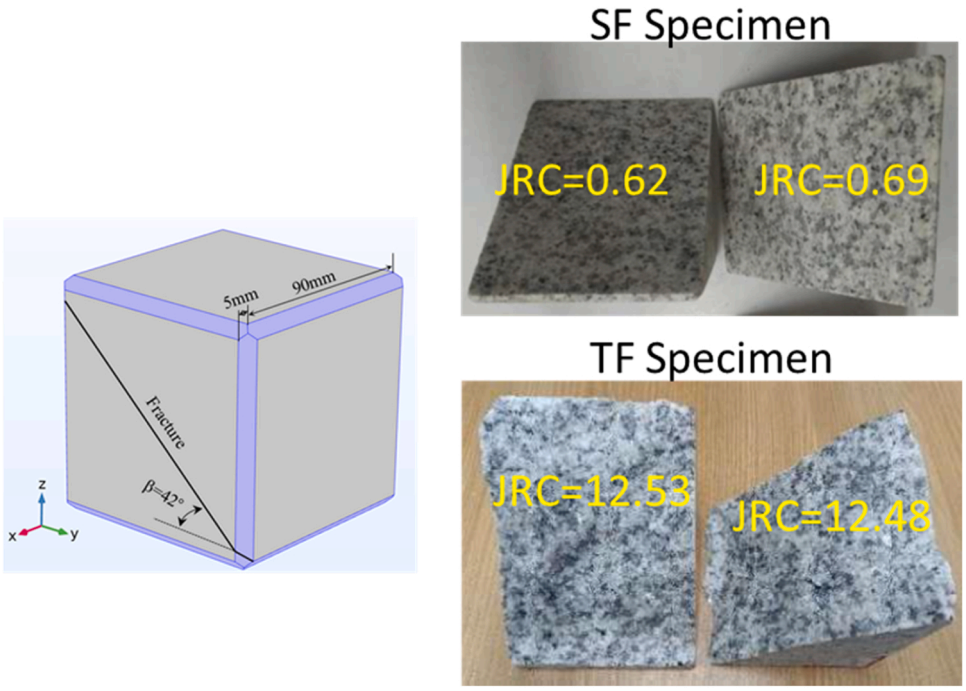

Fig. 7. Fractured Pocheon granite specimens (adapted from[25]. The SF specimen was saw-cut while the TF specimen was created by tension split.

$$|\tau| + \sigma \tan(-\alpha + \varnothing) = 0 \quad when\ \sigma \sin\alpha + \tau \cos\alpha \leq 0 \tag{8.b}$$

Then, by comparing Eqs. (8) and (3), the asperity angle can be expressed as a function of JRC and JCS as:

$$\alpha = JRC \quad Log_{10}\left(\frac{JCS}{\sigma}\right) \tag{9}$$

The surface asperities of real joints, as shown for example in Fig. 3 for a joint in Freiberg granite[23], do not follow a regular pattern with a constant inclination angle α. Several orders of irregularities in the joint surface exist, each order of irregularity being activated depending on the size of the sample. Therefore, Eq. (9) is a simplified conceptualization that provides an "effective" asperity angle that depends on the scale of the joint. The following empirical expression for JRC and JCS that takes into account scale effects could be used:[13,19–21].

$$JRC = JRC_0\left(\frac{L}{L_0}\right)^{-0.02JRC_0} \tag{10}$$

$$JCS = JCS_0\left(\frac{L}{L_0}\right)^{-0.03JCS_0} \tag{11}$$

Where: JRC_0 and JCS_0 are laboratory scale values of joint roughness and compressive strength, for nominal size L_0= 100 mm, and JRC and JCS are values for joint size L.

2.3. Asperity degradation

During the shearing process, the joint surface can be damaged. To account for this damage, following Plesha[10], we assumed that the effective asperity angle degrades according to:

$$\alpha = \alpha_0 e^{-cW_p} \tag{12}$$

where α_0 is the initial effective asperity angle, that can be estimated from the initial JRC as in Eq. (9), c is an asperity degradation constant and W_p is the plastic work induced by shear, per unit area of the joint surface, and accumulated at time t:

$$W_p = \int_0^t \tau \frac{du_p}{dt} dt \tag{13}$$

The constant c is dependent on the normal stress[11]. In this work, we use a calibration procedure using shear tests under constant normal stress in order to determine c.

2.4. Finite element implementation and verification

The joint model was implemented in the commercial general-purpose finite element software COMSOL Multiphysics, Version. 6.1[22]. The Solid Mechanics module was used and the joint was represented by spring interfaces between solid elements, with the rate of plastic relative displacement in equation[6] defined as a "pre-deformation" of the interface. The accumulated plastic relative displacement is calculated by performing time integration of the rate (cf. Eq. 6) using the Boundary Ordinary Differentiation (ODE) module and fully coupling it to the Structural Mechanics module.

The implementation was verified for the case of joint shearing under constant normal load as illustrated in Fig. 4. In this example, the jointed rock sample was sheared to a total relative shear displacement of 0.002 m (2 mm), under a constant normal stress of 1 MPa. The effective asperity angle was set to 33.4°, the friction angle 34°. The shear stiffness was set to 9 GPa/m. The normal stiffness was defined as a smooth step function that varies from zero, when the joint normal displacement exceeds 0.5 μm in tension, and to a stiffness equivalent to the one of the intact rock (8740 GPa/m) when the joint normal displacement exceeds 0.5 μm in compression. The above values are intentionally chosen as the same for the joint in Freiberg granite discussed next.

When no joint degradation is considered, an analytical solution for the joint behaviour can be derived, as follows:

$\tau_{peak} = \sigma \tan(\alpha_0 + \phi) = 2.4$ MPa.

$u_{peak} = \tau_{peak} / k_s = 0.00026$ m (0.26 mm).

$u_p = u - u_{peak} = 0.00174$ m (1.74 mm).

$v_p = u_p \tan(\alpha) = 0.001147$ m(1.147 mm).

$W_p = \tau_{peak} u_p$.

The finite element results are compared to the analytical solution in Fig. 5, showing good albeit not perfect agreement. This is because the

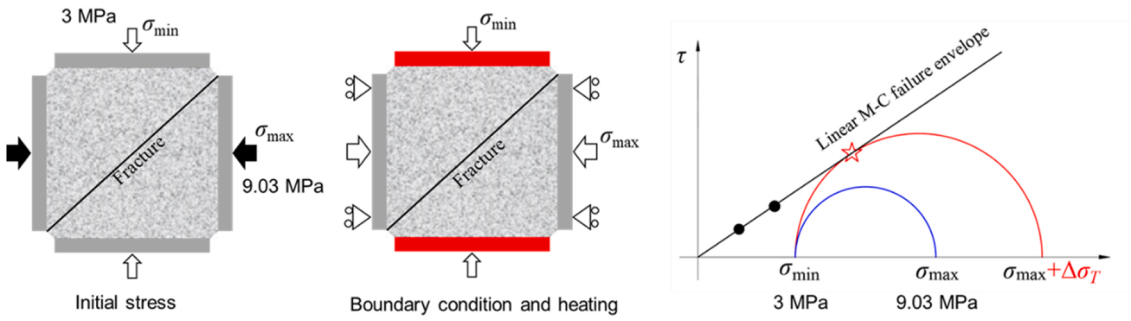

a) Experimental procedure b) Inferred fracture stress

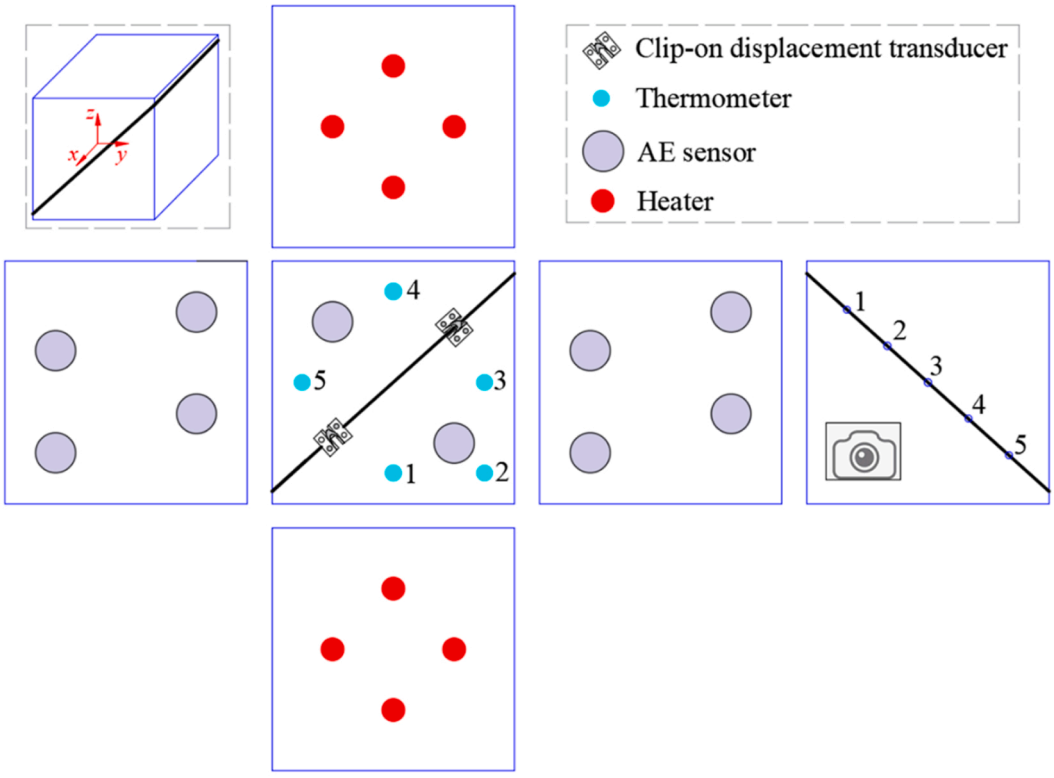

c) Monitoring sensors

Fig. 8. Experimental and monitoring procedures for thermal slip experiments on Pocheon fractured granite (adapted from[25])

analytical solution is applicable to a point-value problem, while the numerical solution is applicable to a boundary value problem, with finite dimensions of the domain being modelled. Displacement and stress conditions from the numerical simulation are not uniform along the fracture. Fig. 5 shows comparison between the value of the relevant variables averaged over the fracture versus the point-value given by the analytical solution. The agreement is deemed acceptable and provides confidence in the implementation of the model in the COMSOL software.

3. Simulation of joint shear under constant normal stress

Here, we validate the proposed joint model with direct shear tests under constant normal stress conducted at the rock mechanics laboratory of the TU Bergakademie Freiberg, Germany[23]. The tests were conducted with a shear box device specially designed at the laboratory[24] on jointed granite and basalt samples. We will focus here on the jointed granite sample. The test configuration is similar to the one for the verification problem shown in Fig. 4b.

The jointed granite sample was sheared under constant normal load of successively 1 MPa, 2.5 MPa, 5 MPa and 7.5 MPa. After the end of each shearing process under a normal load, the joint surfaces were reset to the initial position before testing to the higher normal load. The investigators[23] performed scanning of the joint surface before the start of the test series (Fig. 3) and after the last shearing test and found evidence of damage of the joint surfaces.

The finite element model for the experiment is similar to the one for the verification problem shown in Fig. 4. The input data used are given in Table 1.

The modelling results are compared to the experimental data in Fig. 6. It is shown that good agreement was obtained between the modelling and the experimental results:

- The shear strength as indicated by the stress-displacement curve increases with the normal stress (Fig. 6.a)

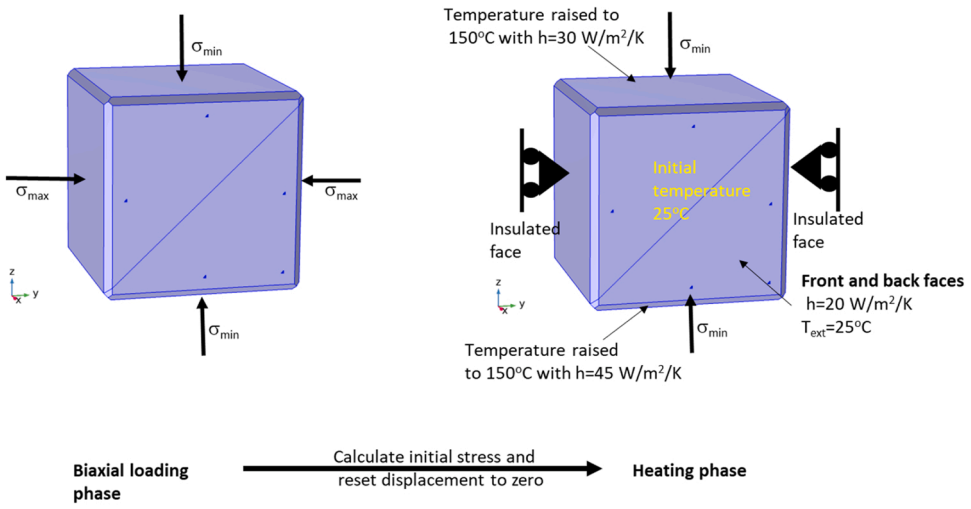

Fig. 9. Finite element model for thermoshearing analysis.

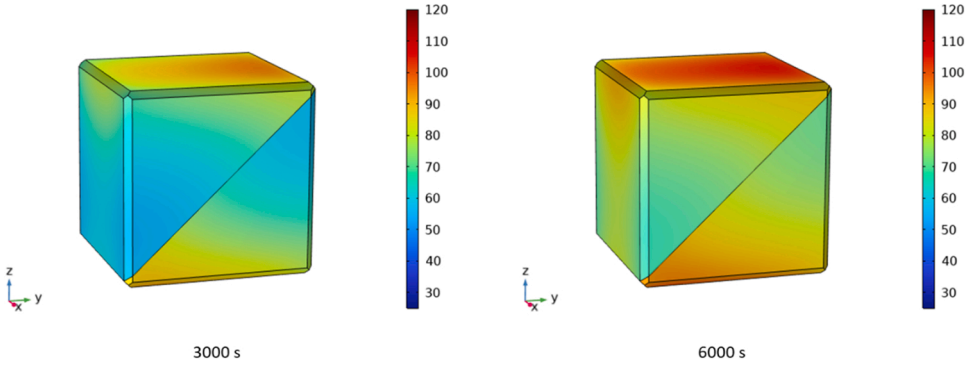

Fig. 10. Modelled temperature (°C) field at 6000 s after heating.

- Joint dilation occurs due to asperity overriding during the shear process (Fig. 6.b). With higher normal stress, dilatancy decreases due to asperity degradation that occurred during the previous shearing phases at lower normal stress. The asperity angle is dependent on the accumulated plastic work as described in Eq. (12). In the numerical simulation, at a certain normal stress level, an initial asperity angle is defined, and then degrades according to Eq. (12). The final value obtained at a normal stress level is used as an initial value in the subsequent analysis at the higher normal stress level.
- At the start of shearing at normal stress of 1 MPa, the JRC was estimated at 16. Consistently with the experimental observation, the model predicts damage of the joint surfaces. The model indicates that JRC decreases to a value of 9.5 at the end of shearing under a normal stress of 7.5 MPa
- As a result of joint asperity degradation, dilation is smaller for tests at higher normal stress (Fig. 6.b). The modelled dilation is consistent with the experimental data for this finding. However, there is some quantitative discrepancy since the model does not account for the initial compression of the joint due to microcracks closing at the beginning of the shearing process.
- Most of the asperity degradation occurred during the first test at 1 MPa normal stress. This is indicated by a pronounced softening behaviour (stress reduction) as shown in Fig. 6.a. For subsequent higher normal stress, the joint exhibited some hardening behaviour followed by a nearly perfectly plastic behaviour. The modelling results are consistent with the experimental data for this softening-hardening behaviour, except for the highest normal stress of 7.5 MPa, where continuous hardening was found.

4. Thermally induced joint shear

4.1. Overview of the experimental procedure

Laboratory experiments to simulate the scenario illustrated in Fig. 1.b were performed on jointed cubes of Pocheon granite of South Korea[25]. The Pocheon granite contains 35.7 % quartz, 35.9 % orthoclase/plagioclase mix, 25.8 % microline and 2.6 % biotite and its thermal and mechanical properties are indicated in Table 2. The three $100\times100\times100$ mm^3 cubes being tested are intersected with fractures oriented at approximately 42° with the horizontal direction. Three types of fractures were created:

- a saw-cut fracture (SF), prepared by cutting through the intact cube with a saw;
- a laser marking fracture (LF), prepared by saw-cutting an intact cube, then shaping the roughness of the top surface by a laser marking machine;
- a tensile splitting fracture (TF), created by splitting the intact cube by tension.

For the LF specimen, there is a strong mismatch between the top and the bottom fracture walls, with estimated JRC of approximately 4 for the top wall and 2 for the bottom wall. We will focus on specimens SF and TF, with matched fracture walls. The SF fracture is smooth, with JRC for bottom and top surfaces estimated respectively at 0.62 and 0.69, while the TF fracture is relatively rough, with JRC values estimated at respectively 12.53 for the top surface, and 12.48 for the bottom surface

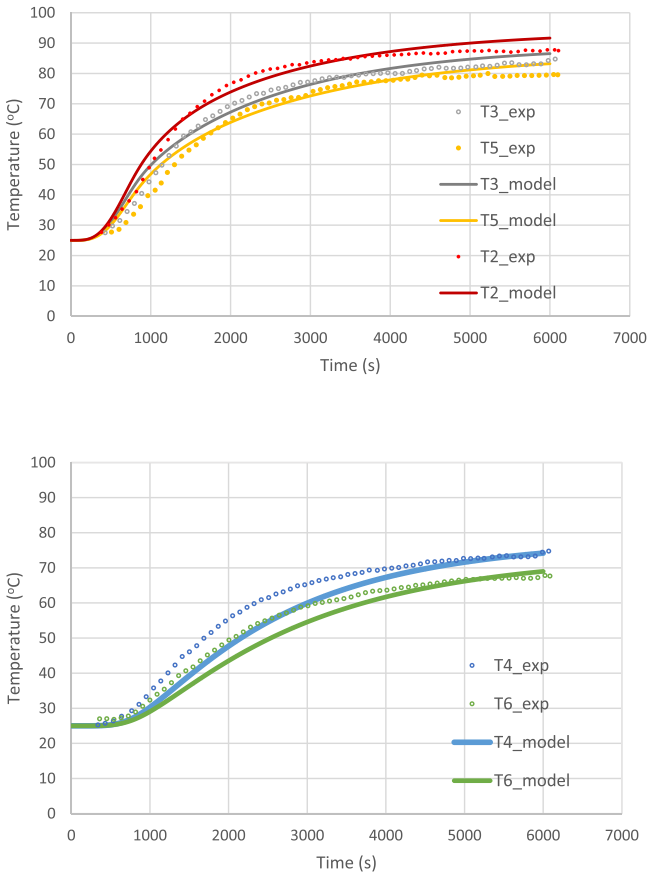

Fig. 11. Temperature evolution on front face of specimen. *Solid lines are modelling results, dots are experimental values.*

(Fig. 7).

The jointed rock specimens were tested in a biaxial apparatus in two phases (Fig. 8):

- First it was compressed with a horizontal stress larger than the vertical stress. The vertical stress was 3 MPa, while the horizontal stress was 9 and 24.61 MPa for the SF and TF samples, respectively (Fig. 8.a)
- Then the horizontal faces are constrained to restrain horizontal displacement, followed by heating from the top and bottom surfaces (Fig. 8.a). Heating would increase the horizontal stress, while the vertical stress remains constant, eventually resulting in slip failure along the fracture when the normal and shear stress on the fracture reach the failure envelope of the fracture (Fig. 8.b). This change in boundary conditions allows higher development of thermal stresses to mimic a bounding scenario for the field conditions as illustrated in Fig. 1.b.
- During the heating phase, temperatures were measured with thermometers emplaced on the outside faces of the cubic sample, shear relative displacements along the fracture were measured by both the clip-on displacement transducers and by camera recordings, and the pressure developed along the restrained vertical faces was recorded by pressure sensors. Acoustic emission was also recorded with AE sensors (Fig. 8.c)

4.2. Modelling procedure and results

The input parameters for the modelling are shown in Table 2. Except for the thermal expansion coefficient, all experimentally determined parameters[25] were directly used as model input. The input value of the coefficient of linear thermal expansion had to be increased from the experimental value, since the latter was obtained from laboratory tests on intact Pocheon granite sample. It is noticed however[25] that the process of fracture creation induced microcracks, and even macrocracks (for the TF) and would lead to an increase in the thermal expansion coefficient. Therefore, for modelling purposes we increase that coefficient by approximately 20 % and 40 % for the SF and TF, respectively.

The finite element model for the thermoshearing experiment showing the sequence, the boundary and initial conditions is illustrated in Fig. 9. In the first phase a steady-state mechanical analysis under a biaxial loading condition was performed. In the second stage, a coupled Thermal-Mechanical transient analysis was performed. In that second phase, the stress distribution calculated from the first phase was input as initial stresses and displacements were re-initialized to zero. The horizontal load was removed and replaced by rollers to prevent normal displacements. Heating was then applied from the top and bottom. Only heat conduction was considered in the thermal process. The initial temperature in the cube and the external temperature were set at 25 °C. The temperature in the heaters at the top and bottom of the specimen was raised to 150 °C within 1000 s. There is heat loss through the heating plates in contact with the specimen. Instead of considering the plates explicitly, we assumed that heat fluxes from the heater into the rock specimen could be represented as:

$$Q_{heater} = h(T\text{-}T_{heater}) \quad (14)$$

where h is a heat transfer coefficient through the plates, calibrated to 45 W/m^2/K and 30 W/m^2/K for the bottom and the top surfaces, respectively and T_{heater} is the heater temperature, being raised from 25 °C to 150 °C in 900 s

The front and back faces are in contact with the open air and heat loss from these faces due to natural convection are simulated as:

$$Q_{conv} = h(T\text{-}T_{ext}) \quad (15)$$

where T is the temperature on the face inside the cube, T_{ext} = 25 °C is the external temperature and h is the heat transfer coefficient, assumed

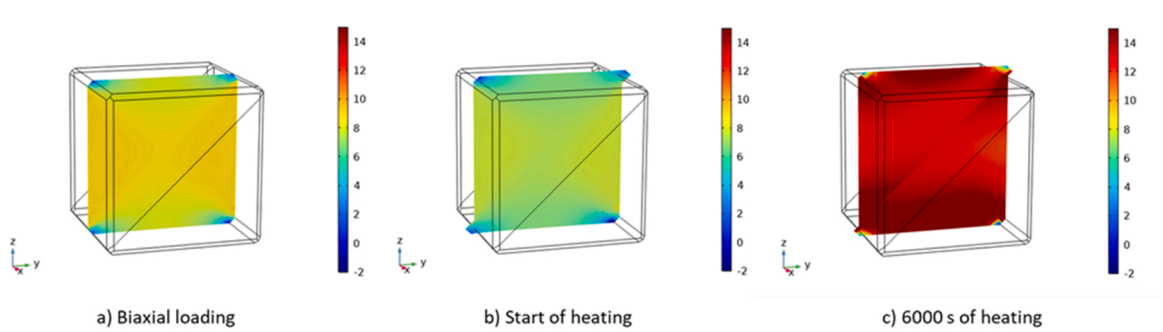

Fig. 12. Horizontal stress (MPa) distribution at different phases of thermoshearing experiment on SF sample.

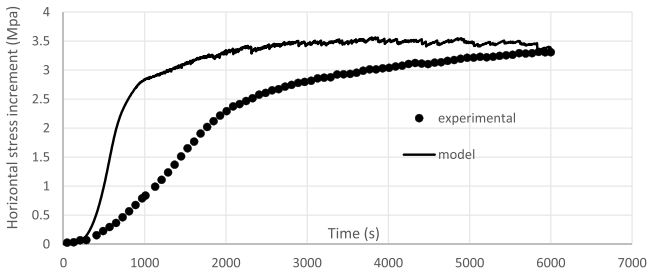

a) Horizontal stress increment

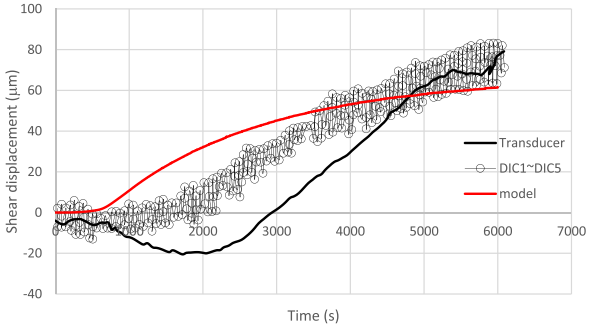

b) Shear displacement

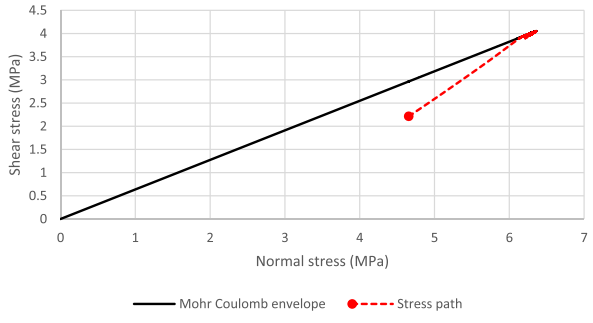

c) Stress path for the fracture

Fig. 13. Horizontal stress increment, shear displacement and stress path for the SF fracture – *Sensors and cameras recording positions are shown in* Fig. 8.*c*.

to be 20 W/m^2/K which is a typical value for still air.

The fracture is assumed to be a thin resisting layer, since as observed during the experiment, the fracture surfaces are not in perfect contact, especially for the TF specimen. The heat transfer flux across the fracture is modelled as:

$$Q=-(T_u-T_d)/R \quad (16)$$

Where T_u and T_d are, respectively, the temperatures on the upper and lower surfaces of the fracture; and R is the heat flux resistance, calibrated to 0.15 K.m^2/W.

Typical output for the temperature field is shown in Fig. 10. The temperature field clearly shows the effect of natural convection at the front and back faces, resulting in lower temperatures on these faces as compared to the interior of the specimen. The temperature field also shows the effects of thermal resistance of the fracture, due to imperfect match between the upper and lower surfaces. For simplification we assumed that the temperature fields would be the same for the SF and TF specimens. The experimental temperature discussed in[25] is reported solely for the SF specimen, implicitly assuming that for the TF specimen, the same temperature field would prevail.

The calculated temperature evolution is compared to the measured evolution at different thermometers (Fig. 8.c) positioned on the front face of the specimen in Fig. 11. The comparison is reasonably good for all positions, considering the uncertainties related to the complex conditions of heat transfer from the heaters, which were not included in the model. The modelling results show that temperatures near the heaters (T2, T4 and T5) are higher than temperatures in the horizontal mid-plane (T3 and T6). It could also be seen that temperatures at T4 and T6 are different, although these sensors are at the same distance from the heaters. This is due to the effect of the fracture. By including a thin resistive layer, this effect is captured by the model.

Fig. 12.a shows the modelled horizontal stress distribution, in the vertical mid-plane of the cubic sample, resulting from the biaxial state of stress σ_{min} on the horizontal faces and σ_{max} on the vertical faces. Due to the presence of the fracture, the stress distribution within the sample is not uniform. This stress distribution was used as the initial stress for the subsequent thermo-mechanical analysis. Before heating started, σ_{max} was removed, and the vertical faces were restrained against normal displacement. This operation would result in a stress relaxation due to some sliding along the fracture, as indicated in Fig. 12.b. Subsequent heating would result in an increase in stresses in the sample, as indicated in Fig. 12.c. The normal and shear stresses along the joint increase simultaneously due to heating, leading to its eventual shear failure.

For the SF specimen, the modelling results for joint displacement and thermally induced horizontal stress increment for the SF specimen are shown in Fig. 13 and compared with the experimental data. Consistently with the experimental observations, as temperature increases the horizontal stress increases on the restrained vertical faces of the sample (Fig. 13a). The incremental stress at equilibrium from the model compares reasonably well with the measured value. However, the model indicates an earlier stress increase as compared to the experimental values. In order to obtain a better agreement of the transient stress evolution, a recalibration of the thermal analysis might be necessary, that would require a more accurate representation of the heating plates and the loading plates. The shear displacement (Fig. 13.b) predicted by the model compares well in trend and absolute values with the recorded data. Shear displacement is minimal up to 1200 s of heating, exhibiting a rigid-plastic behaviour. The normal and shear stress in the joint increase simultaneously due to heating, eventually reaching the yield conditions as conceptualized in Fig. 7.b and shown in Fig. 13.c. For the SF specimen, modelled joint dilation is very small of the order of 1–2 μm as also recorded from the experiment.

For the TF specimen, the modelling results also compare well with the experimental values for shear displacements (Fig. 14.a) as measured by the transducer and camera recordings at most positions. For dilation, the modelled results also compared well with the camera recordings. The measurement of dilation from the sensor (Fig. 14.b) is however unreliable, since it was reported that it experienced thermal expansion during the heating process. As compared to the SF specimen, shear displacement is larger, mainly due to the larger asperity degradation, as discussed below. The fracture dilation is also larger due to the more pronounced roughness of the fracture surface.

The modelled horizontal stress, consistently with the experimental measurement, shows first an increase followed by a decrease (Fig. 15). However, the timing and absolute values of the modelled stress increments do not match well with the experimental values. The modelled stress decrease is due to strain softening triggered by the asperity damage that reduces the value of the effective asperity angle, as shown in Fig. 15. This is consistent with the post-test observations by Zhuang et al[20]. who reported sheared off particles from the fracture walls. In addition, these authors also reported microcracks and localized macrocracks forming from the main fracture. Crack propagation into the rock matrix will make the overall strain softening more pronounced and this phenomenon is not included in the current model, where the rock matrix is assumed to be linear elastic.

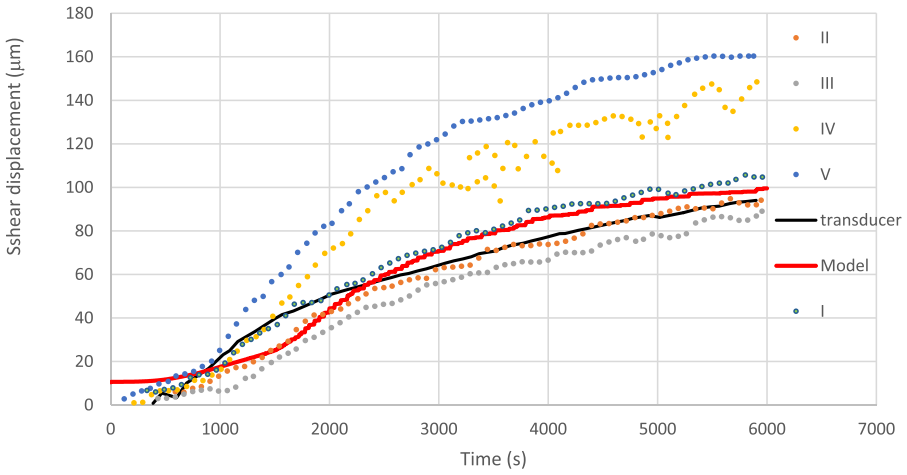

a) Shear displacement

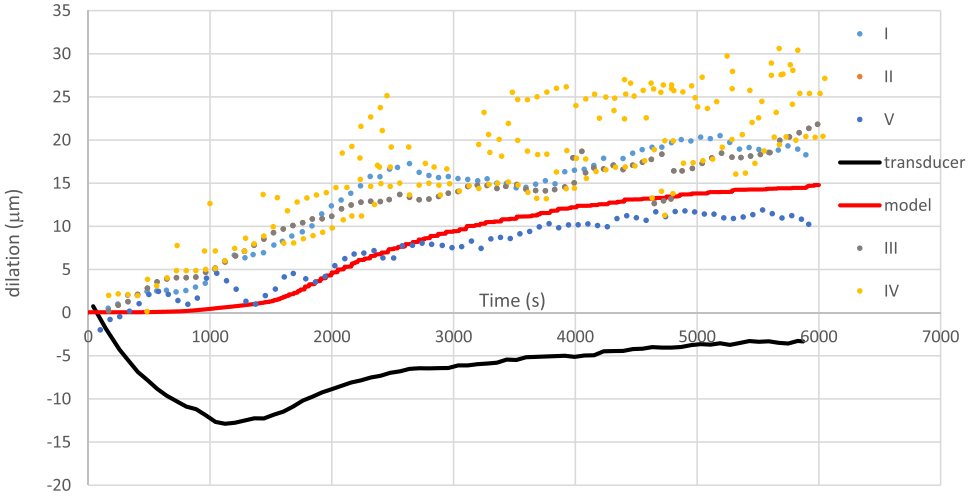

b) Dilation

Fig. 14. Shear and dilation displacement for TF fracture - Sensors and cameras recording positions are shown in Fig. 8.c.

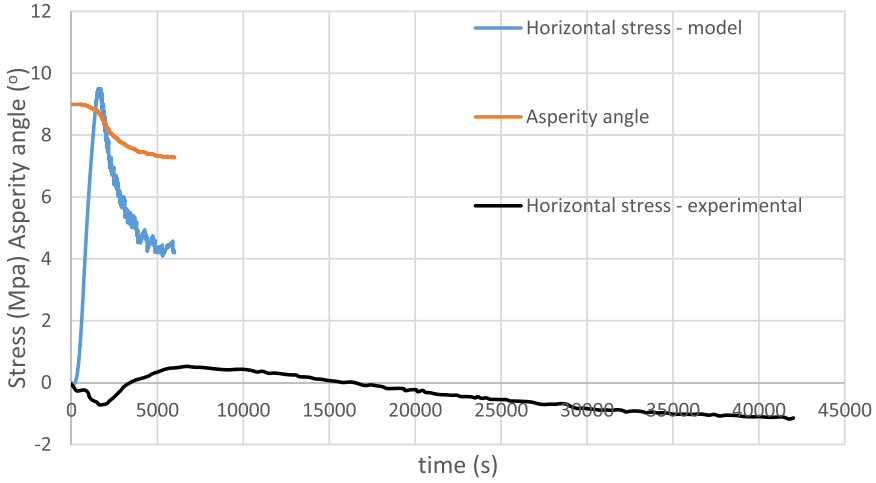

Fig. 15. Modelled horizontal stress increment and asperity damage for TF specimen.

5. Conclusions

A DGR for the disposal of radioactive waste, in addition to the engineered components, relies on the rock to contain and isolate the waste for very long periods of time. Rock masses at the depth of a typical DGR would in general comprise intact rock, discrete joints, and major fault zones. Major faults and discrete joints are planes of weakness in the rock mas and can be preferential pathways for radionuclide migrations. The DGR should be located away from the major faults, and waste emplacement should avoid as much as possible locations of high-intensity jointing. However, due to the extensive footprint of the DGR, undetected joints might occur in the emplacement location of a waste container. Under different external events and internal processes, the joint can shear, and potential excessive shear movements can affect the structural integrity of the container and the bentonite seals. Furthermore, dilation that accompanies shear of rough joints would increase its hydraulic aperture and further enhance its potential for radionuclide transport. Therefore, for the long-term safety assessment of a DGR, the situation of an undetected joint crossing the emplacement of a waste container should be evaluated, and the implications of this situation need to be integrated in the safety assessment and design of the DGR. Mathematical models are powerful tools that could be used to evaluate the safety implications of the above scenario.

In this paper, we developed and validated such a model. The model input uses two main parameters, JRC and JCS, which could be measured from inexpensive standard tests commonly conducted in rock engineering. The model was shown to be able to reproduce the main physical processes in two sets of laboratory tests. The first set of tests was shearing tests of jointed Freiberg granite, under constant normal loads. The model successively reproduced the increased strength and decreased dilation with increasing normal loads, and joint asperity damage induced by shear. The second set of tests is thermal shearing experiments conducted on Pocheon granite specimens with inclined fractures. The specimens were first loaded to simulate a biaxial state of stress near the slip conditions. Subsequently, the specimens were restrained by the sides and heated from the top and bottom, resulting in change of stress conditions within the fracture that trigger its slip. The model successfully predicted the temperature evolution in the specimens, and the thermally induced stress conditions that led to the fracture slip and its subsequent pronounced shear displacement. Two fracture types were considered: a smooth fracture and a rough fracture. For the smooth fracture, minimal dilation was predicted consistently with the experiment finding. For the rough fracture, also consistently with the experimental findings, more pronounced dilation and asperity damage were predicted. Damage induced stress relief, as predicted by the model, and observed from the experiment. However, the modelled stress relief does not match well in absolute value and timing with the experimental data. Experimental observations showed that damage occurred not only to the fracture asperities, but also propagated into the rock matrix in the form of microcracks and localized macrocracks. The latter process is recommended for future investigations. In addition to the effects of rock matrix damage and fracture propagation into the rock matrix, future investigations would include the effects of pore pressure (e.g. THM coupling) and the effects of different stress paths (e.g. shear under constant normal stiffness). These investigations are being planned for the next phase of DECOVALEX. The current model seems to have the potential to be further developed and validated with the new experimental data that would become available.

CRediT authorship contribution statement

Nguyen Son Thanh: Conceptualization, Formal analysis, Funding acquisition, Investigation, Methodology, Resources, Software, Writing – original draft, Writing – review & editing. **Kolditz Olaf:** Data curation, Funding acquisition, Project administration, Validation, Writing – review & editing. **Zhuang Li:** Data curation, Validation, Writing – review & editing. **Yoon Jeoung Seok:** Data curation, Project administration, Validation, Writing – review & editing.

Declaration of Competing Interest

The authors declare that they have no known competing financial interests or personal relationships that could have appeared to influence the work reported in this paper.

Data availability

Data will be made available on request.

Acknowledgements

DECOVALEX is an international research project comprising participants from industry, government and academia, focusing on development of understanding, models and codes in complex coupled problems in sub-surface geological and engineering applications; DECOVALEX-2023 is the current phase of the project. The authors appreciate and thank the DECOVALEX-2023 Funding Organisations Andra, BASE, BGE, BGR, CAS, CNSC, COVRA, US DOE, ENRESA, ENSI, JAEA, KAERI, NWMO, NWS, SÚRAO, SSM and Taipower for their financial and technical support of the work described in this paper. The statements made in the paper are, however, solely those of the authors and do not necessarily reflect those of the Funding Organisations. Sincere appreciation is also acknowledged for TU Freiberg, Institut fur Geotechnik (contributors Frühwirt T, Pöetschke D) for providing the experimental data of the shearing tests of the joint in Freiberg granite.

References

1. Shukla R, Ranjith P, Haque A, Cho X. A review of studies on CO_2 sequestration and caprock integrity. *Fuel*. 2010;89:2651–2664.
2. Zoback MD, Gorelick SM. Earthquake triggering and large-scale geologic storage of carbon dioxide. *Proc Natl Acad Sci*. 2012;109(26):10164–10168.
3. Rutqvist J., Rinaldi A.P., Cappa F. and Moridis G.J. Modeling of fault activation and seismicity by injection directly into a fault zone associated with hydraulic fracturing of shale-gas reservoirs. J Pet Sci Eng 2015; 127: 377–386.
4. Xie L. and Min K.B. Hydraulic fracturing initiation and propagation in deep inclined open hole for Enhanced Geothermal System. Geothermics 2017; 70: 351–366.
5. De Simone S., Carrera J. and Vilarrasa V. Superposition approach to understand triggering mechanisms of post-injection induced seismicity. Geothermics 2017; 70: 85–97.
6. SKB (Swedish Nuclear Fuel and Waste Management Co.). Post-closure safety for the final repository for spent nuclear fuel at Forsmark - Main report, PSAR version. SKB TR-21–01 2022. https://www.skb.com/publication/2506409/TR-21–01.pdf.
7. Birkholzer JT, Tsang C, Bond A, Hudson AJ, Jing L, Stephansson O. 25 years of DECOVALEX - Scientific advances and lessons learned from an international research collaboration in coupled subsurface processes. *Int J Rock Mech Min Sci Geomech Abst.* 2019;122:1053995. https://doi.org/10.1016/j.ijrmms.2019.03.015.
8. Nguyen TS. Thermo-Hydro-Mechanical-Chemical processes in geological disposal of radioactive waste – An example of regulatory research. *Adv Geo-Energy Res*. 2018;2 (2):173–189. ⟨https://www.yandy-ager.com/index.php/ager/article/view/28⟩.
9. Patton F.D. Multiple modes of shear failure in rock. Proc. 1st Congress of Int. Society of Rock Mech., Lisbon. 1966; 1:509–513.
10. Plesha ME. Constitutive models for rock discontinuities with dilatancy and surface degradation. *Int J Numer Anal Meth Geomech*. 1987;11:345–362.
11. Benjelloun Z.H. Étude Expérimentale et Modélisation du Comportement Hydromécanique des Joints Rocheux. Thèse de doctorat, Université Joseph Fourier, Grenoble 1.1993.
12. Ladanyi B. and Archambault G. Simulation of shear behaviour of a jointed rock mass. Proc. 11th Symp. Rock.Mech. American Institute of Mechanical Engineers, New York. 1970.
13. Barton N, Choubey V V. The shear strength of rock joints in theory and practice. *Rock Mech*. 1977;10:1–54.
14. Heuze FE, Barbour TG. New models for rock joints and interfaces. *J Geotechn Eng, Div Proc ASCE*. 1982;108:757–776.
15. Nguyen TS, Selvadurai APS. *A model for coupled hydraulic and mechanical behaviour of a rock joint*. In: *Int. J. Num.An. Meth. Geom*. 22. 1998:29–48. ⟨https://onlinelibrary.wiley.com/doi/10.1002/(SICI)1096-9853(199801)22:1%3C29::AID-NAG907%3E3.0.CO;2-N⟩.
16. Michalowski R, Mroz Z. Associated and non-associated sliding rules in contact friction problems. *Arch Mech*. 1978;30:259–276.
17. Mollaali M, Kolditz O and al. Comparative verification of hydro-mechanical fracture behavior: Task G of international research project DECOVALEX–2023. *Int J Rock*

Mech Min Sci Geomech Abst. 2023;170, 105530. https://doi.org/10.1016/j.ijrmms.2023.105530.
18. Zienkiewicz OC, Cormeau IC. Visco-plasticity—plasticity and creep in elastic solids—a unified numerical solution approach. *Int J Num Meth Eng.* 1974;8:821. https://doi.org/10.1002/nme.1620080411.
19. Bandis S, Lumsden AC, Barton N. Experimental studies of scale effects on the shear behaviour of rock joints. *Int J Rock Mech Min Sci Geomech Abst.* 1981;18:1–21.
20. Barton N, Bandis S, Bakhtar K. Strength, deformation and conductivity coupling of rock joints. *Int J Rock Mech Min Sci Geomech Abstr.* 1985;22(3):121–140.
21. Barton N. Barton-Bandis criterion. *Encycl Eng Geol.* 2018:1–9.
22. COMSOL. Introduction to COMSOL Multiphysics 1998-202. https://www.comsol.com/documentation.
23. Frühwirt T, Pöetschke D, Konietzky H. Simulation of direct shear tests using a Forces on Fracture Surfaces (FFS) approach. *Env Earth Sci.* 2021;80, 312. https://doi.org/10.1007/s12665-021-09606-6.
24. Konietzky H, Frühwirt T, Luge H. A new large dynamic rock mechanical direct shear box device. *Rock Mech Rock Eng.* 2012;45(3):427–432. https://doi.org/10.1007/s00603-011-0214-x.
25. Sun C, Zhuang L, Yoon JS, Min KB. Thermally induced shear reactivation of critically-stressed smooth and rough granite fractures. *IOP Conf Ser: Earth Environ Sci.* 2023;1124, 012119. https://doi.org/10.1088/1755-1315/1124/1/012119.
26. Sun C, Zhuang L, Jung S, Lee J, Yoon YS. Thermally induced slip of a single sawcut granite fracture under biaxial loading. *Geomech Geophys Geo-Energ Geo-Resour.* 2021;7(4):1–13. https://doi.org/10.1007/s40948-021-00293-y.